Available online at www.sciencedirect.com
SCIENCE DIRECT®
Journal of Molecular Catalysis A: Chemical 208 (2004) 55–65
JOURNAL OF MOLECULAR CATALYSIS A: CHEMICAL
www.elsevier.com/locate/molcata

Effect of "topotactic" reduction product of tungsten disulfide on catalytic activity of metallocene catalyst for olefin polymerization

Satoru Yamada [a,b], Akihiro Yano [b], Morihiko Sato [b], Takahito Itoh [a,*]

[a] *Department of Chemistry for Materials, Faculty of Engineering, Mie University, 1515 Kamihama-cho, Tsu-shi, Mie 514-8507, Japan*
[b] *Yokkaichi Research Laboratory, TOSOH Corporation, 1-8 Kasumi, Yokkaichi, Mie 510-8540, Japan*

Received 21 February 2003; received in revised form 14 May 2003; accepted 14 July 2003

Abstract

N,*N*-Dimethylanilinium ($Ph(Me)_2NH^+$) salt of tungsten disulfide (WS_2) was developed as a novel cocatalyst for metallocene catalysts. The cocatalyst is composed of *N*,*N*-dimethylanilinium ion as a cationic part and "topotactic" reduction product of WS_2, obtained by acquisition of an electron by the neutral host lattice of WS_2 without structural alteration, as an anionic part. Notable improvement of the catalytic activity for ethylene polymerization using the bis(indenyl)zirconium dichloride (Ind_2ZrCl_2)/triethylaluminum (Et_3Al) catalyst was observed upon the addition of the $Ph(Me)_2NH^+$ salt of WS_2. The addition of the corresponding molybdenum disulfide (MoS_2) one that had smaller crystallite size than the $Ph(Me)_2NH^+$ salt of WS_2 showed the lower catalytic activity. The resultant poly(ethylene) prepared by the $Ind_2ZrCl_2/Et_3Al/Ph(Me)_2NH^+$ salt of WS_2 possessed similar properties like narrow polydispersity to that prepared by conventional metallocene type catalysts. The Zr loadings on the precipitate of the Ind_2ZrCl_2/Et_3Al catalyst activated by the $Ph(Me)_2NH^+$ salt of WS_2 increased with a decrease in the crystallite size of the $Ph(Me)_2NH^+$ salt of WS_2. However, the catalytic activities in ethylene polymerization decreased drastically, indicating that the decrease of the crystallite size led to the significant increase of inactive species for ethylene polymerization.

Keywords: Cocatalyst; *N*,*N*-Dimethylanilinium salt; Tungsten disulfide; Metallocene catalyst; Polymerization; Topotactic reduction

1. Introduction

Metallocene/alkylaluminum catalysts have long been employed as a model of heterogeneous Ziegler–Natta polymerization catalysts for mechanistic studies [1]. However, this metallocene catalyst has not attracted much attention because of its poor catalytic activity. Accidental observation that moisture significantly improved the catalytic activity of group 4 metallocene derivatives, for example, bis(cyclopentadienyl)zirconium(IV) dimethyl (Cp_2ZrMe_2)/alkylaluminum, in ethylene and propylene polymerizations led to a discovery of methylaluminoxane (MAO) as a cocatalyst [1,2]. This finding aroused commercial and scientific interests in the metallocene catalyst. It has been proposed that in these polymerizations MAO as a Lewis acid might abstract an alkyl group to form a formally three-coordinate cation, i.e., $[Cp_2ZrMe^+]$ [3,4]. The formation of such a cationic metallocene compound stimulated researchers to investigate the ionic compounds of the $[Cp'_2MR^+][A^-]$ type, where Cp′, M, R, and A^- are a substituted or unsubstituted cyclopentadienide, a group 4 metal, an alkyl group, and a counter anion, respectively, and it was found that the activity of these compounds was highly sensitive to the nature of the counter anion. When hexafluorophosphate (PF_6^-) or tetraphenylborate (BPh_4^-) was used as a counter anion for "naked" Cp'_2MR^+ cation, anion degradation [5] or poor anion lability [6] was observed. On the other hand, the Cp'_2MCl_2/alkylaluminum catalyst activated with a tetrakis(pentafluorophenyl)borate ($B(C_6F_5)_4^-$)-based salt was reported to be as active as the Cp'_2MR_2/MAO catalyst [7,8]. The $B(C_6F_5)_4^-$-based salt as a cocatalyst has been shown to convert Cp'_2MR_2 into the Cp'_2MR^+ by protonolysis or alkyl abstraction and to provide the cationic species with $B(C_6F_5)_4^-$ as a non-coordinating anion [8–10]. The active species in the Cp'_2MCl_2/alkylaluminum catalyst activated with $B(C_6F_5)_4^-$-based salt was supposed to be a salt of Cp'_2MR^+ with $B(C_6F_5)_4^-$ [8]. Previously, we reported that the salt of ammonium ion and anion obtained by

* Corresponding author. Tel.: +81-59-231-9410; fax: +81-59-231-9410.
E-mail address: itoh@chem.mie-u.ac.jp (T. Itoh).

1381-1169/$ – see front matter © 2003 Elsevier B.V. All rights reserved.
doi:10.1016/j.molcata.2003.07.011

"topotactic" reduction, the principle of which is defined in detail by Schöllhorn [11], acts as an effective cocatalyst for metallocene catalysts in the ethylene polymerization [12]. Recently, we found that in ethylene polymerization using the Cp'_2MCl_2/alkylaluminum catalyst activated with cocatalyst obtained by "topotactic" reduction of molybdenum disulfide (MoS_2) as a two-dimensional host lattice system, the catalytic activity increases with an increase in the amount of ammonium ion present in the interlayer spaces of MoS_2 and suggested that the ammonium ion on the edges of layered structure of MoS_2 would react with a neutral Cp'_2MR_2 to form Cp'_2MR^+ as a cationic species (protonolysis) and a two-dimentional macroanion ($[MoS_2]^{x-}$) as a non-coordinating anion [13]. We are interested in a cocatalyst as a two-dimensional host lattice system other than MoS_2-based cocatalyst and the influence of the crystallite size of cocatalysts on the catalytic activity in the ethylene polymerization.

In this paper, a cocatalyst based on tungsten disulfide (WS_2) as a two-dimensional host lattice system was synthesized, and the effect of the cocatalyst on catalytic activity of a metallocene catalyst and the influence of crystallite size of the cocatalyst in the ethylene polymerization were studied in comparison with the MoS_2-based cocatalyst.

2. Experimental

2.1. Materials

Tungsten disulfide (WS_2) (99.8%, Soekawa Chemicals Co.), *n*-butyllithium (BuLi) solution in *n*-hexane (1.6 mol l^{-1}, Kanto Chemicals Co.), 25% (13 mol l^{-1}) aqueous ammonia (Wako Pure Chemical Industries, Ltd.), triethylaluminum (Et_3Al) solution in toluene (20 wt.%, TOSOH Fine Chemicals Co.), toluene (Kanto Chemicals Co.), and ethylene (purity 99.99%, produced by Sumitomo Seika Co.) were used without further purification. *N*,*N*-Dimethylanilinium chloride ($Ph(Me)_2N{\cdot}HCl$) was prepared by addition of hydrogen chloride to *N*,*N*-dimethylaniline in diethyl ether. *N*,*N*-Dimethylanilinium ion ($Ph(Me)_2NH^+$) intercalated molybdenum disulfide ($[Ph(Me)_2NH^+]_z$ $[MoS_2]^{z-}$) (MON-1) was prepared according to the procedure reported previously at the conditions of [MoS_2], 0.1 mol l^{-1}; [BuLi], 0.2 mol l^{-1}; temperature, 20 °C; time, 18 h for the topotactic reduction; [NH_3], 13 mol l^{-1}; temperature, −30 °C; time, 3 h for the hydration; [$Ph(Me)_2N{\cdot}HCl$], 0.2 mol l^{-1}; temperature, 20 °C; time, 18 h for the ion exchange [13]. Bis(indenyl)-zirconium dichloride (Ind_2ZrCl_2) was synthesized according to the procedure reported in [14].

2.2. N,N-Dimethylanilinium ion intercalated WS_2

N,*N*-Dimethylanilinium ion ($Ph(Me)_2NH^+$) intercalated WS_2 ($[Ph(Me)_2NH^+]_z[WS_2]^{z-}$) was prepared in the procedure similar to that of MON-1. The preparation of typical compound (TUN-1) is shown below. WS_2 powder was soaked at the concentration of 0.3 mol l^{-1} in BuLi solution (1.6 mol l^{-1}) in hexane under nitrogen atmosphere for 18 h at a temperature of 108 °C to give a Li^+ intercalated WS_2 (Li_xWS_2), which was collected by filtration, washed repeatedly with *n*-hexane, and then dried at room temperature under reduced pressure until a constant weight is obtained [15]. Then, the resulting Li_xWS_2 powder was soaked in aqueous ammonia (13 mol l^{-1}) under nitrogen atmosphere for 30 min at a temperature of −30 °C and then washed with water to give the corresponding hydrated product ($(Li^+)_{x-m}(H_2O)_y[WS_2]^{(x-m)-}$), which was collected by filtration [16]. The obtained hydrates were soaked in aqueous $Ph(Me)_2N{\cdot}HCl$ solution (0.2 mol l^{-1}) under nitrogen atmosphere for 18 h at 20 °C. The deposited product ($[Ph(Me)_2NH^+]_z[WS_2]^{z-}$) was collected, washed repeatedly with water, and dried at room temperature under reduced pressure until a constant weight is obtained.

2.3. Supported Ind_2ZrCl_2/Et_3Al catalyst on $[Ph(Me)_2NH^+]_z[WS_2]^{z-}$

In a 100 ml Schlenk tube, a slurry of $[Ph(Me)_2NH^+]_z$ $[WS_2]^{z-}$ in 100 ml of toluene was treated with 0.7 ml of Et_3Al solution in toluene (1.0 mmol) and stirred for 1 h at room temperature. In another Schlenk tube, 3.9 mg (10 μmol) of Ind_2ZrCl_2 was dissolved in 6.4 ml of toluene, treated with 1.4 ml of Et_3Al solution in toluene (2 mmol), and stirred for 30 min at room temperature. Then, this solution was added to the above slurry. The mixture was stirred for 18 h at room temperature, allowed to stand for 3 days, and then the supernatant was removed by a cannula. The precipitate was washed with 100 ml of hexane and dried at room temperature under reduced pressure until a constant weight was obtained.

2.4. Procedure for ethylene polymerization with the Ind_2ZrCl_2/Et_3Al catalyst activated with $[Ph(Me)_2NH^+]_z[WS_2]^{z-}$

In a Schlenk tube, a slurry of $[Ph(Me)_2NH^+]_z[WS_2]^{z-}$ in 10 ml of toluene was treated with 0.07 ml of Et_3Al solution in toluene (100 μmol) and stirred for 1 h at room temperature. In another Schlenk tube, 3.9 mg (10 μmol) of Ind_2ZrCl_2 was dissolved in 6.4 ml of toluene, treated with 1.4 ml of Et_3Al solution in toluene (2 mmol), and stirred for 30 min at room temperature. Then, 0.78 ml of this solution was added to the above slurry. The mixture was stirred for 18 h at room temperature and added to a solution of 500 ml of toluene and 0.14 ml of Et_3Al solution in toluene (200 μmol) in a 1 l Schlenk tube. The mixture was then transferred into a 2 l stainless steel autoclave equipped with a magnetic stirrer, a thermometer, an inlet tube, and an external jacket heated at 80 °C. Ethylene was immediately introduced up to 2.0 MPa or 0.6 MPa of partial pressure. Ethylene was continuously supplied into the autoclave to keep the pressure constant

during polymerization. Internal temperature of the autoclave was kept at 80 °C by the external jacket during polymerization. After a given polymerization time, ethanol was added to the reaction mixture to stop the polymerization and then unreacted ethylene gas was released to leave polymer, which was adequately washed with excess amount of ethanol and dried at 70 °C under reduced pressure until a constant weight was obtained.

2.5. Procedure for ethylene polymerization with the supported Ind_2ZrCl_2/Et_3Al catalyst on $[Ph(Me)_2NH^+]_z[WS_2]^{z-}$

Polymerization was carried out in a procedure similar to that for the Ind_2ZrCl_2/Et_3Al catalyst activated with $[Ph(Me)_2NH^+]_z[WS_2]^{z-}$, except for using a slurry of the supported Ind_2ZrCl_2/Et_3Al catalyst on $[Ph(Me)_2NH^+]_z[WS_2]^{z-}$ in 10 ml of toluene treated with 0.07 ml of Et_3Al solution in toluene (100 μmol).

2.6. Characterization

X-ray diffraction (XRD) measurements of $[Ph(Me)_2NH^+]_z[WS_2]^{z-}$ and $(Li^+)_{x-m}(H_2O)_y[WS_2]^{(x-m)-}$ were performed on a Mac Science MXP18VA diffractometer using Cu Kα radiation (40 kV, 150 mA) at an instrumental resolution of 0.02° in 2θ and a scanning rate of 2° min^{-1}. The $Ph(Me)_2NH^+$ content of $[Ph(Me)_2NH^+]_z[WS_2]^{z-}$ was determined by CHN analysis (Yanaco CHN CORDER MT-5). The BET surface area was measured by nitrogen physisorption at 77 K (Micromeritics ASAP 2400, manufactured by Shimadzu Co.). X-ray photoelectron spectroscopy (XPS) was performed on a X-probe Model 101 spectrometer (Surface Science Instruments, VG Fisons) using a monochromatized Mg Kα X-ray source. The W and Zr contents of the supported Ind_2ZrCl_2/Et_3Al catalyst on $[Ph(Me)_2NH^+]_z[WS_2]^{z-}$ were measured by inductively coupled plasma (ICP) atomic emission spectrophotometer (DERIVATIVE ICPAES UOP-1 (M) MK-II, manufactured by KYOTO-KOKEN Inc.). Molecular weight distribution of the polymer were measured on a gel permeation chromatography (GPC) apparatus (Waters Model 150 C ALC/GPC) with a column GMH-HR-H (S) (TOSOH Corporation) at 145 °C, calibrated with standard polystyrene as a reference, with *o*-dichlorobenzene as an eluent.

3. Results and discussion

3.1. Preparation and characterization of the *N,N*-dimethylanilinium ion intercalated WS_2

Intercalation of *N,N*-dimethylanilinium ion ($Ph(Me)_2NH^+$) into interlayer spaces of the WS_2 was carried out following the procedure for the preparation of $Ph(Me)_2NH^+$ intercalated MoS_2 ($[Ph(Me)_2NH^+]_z[MoS_2]^{z-}$) shown in Scheme 1 [13,15].

The topotactic reduction of WS_2 and MoS_2 with BuLi gave Li^+ intercalated WS_2 (Li_xWS_2) and MoS_2 (Li_xMoS_2), respectively. The Li^+ present in interlayers of the Li_xWS_2 was hydrated by the treatment of Li_xWS_2 with aqueous ammonia for 30 min at −30 °C, followed by the treatment of water [16]. The X-ray powder diffraction pattern of pure WS_2 is shown in Fig. 1(a), where the peaks of $2\theta = 14.08$, 28.64, and 43.70° are assignable to 0 0 1, 0 0 2, and 0 0 3 reflections, respectively.

The basal spacing (*d*), that is, the distance between neighboring WS_2 layers was 6.28 Å, calculated by the Bragg's formula, d (Å) $= \lambda$ (=1.5405 Å)/2 sin θ, and $2\theta = 14.08°$ at the 0 0 1 reflection, identical to the value (6.24 Å) reported by Whittingham [17]. The XRD pattern of the hydration product in a wet state is shown in Fig. 1(b), where the peaks of $2\theta = 6.86°$, 14.08, and 21.30 are assignable to 0 0 1, 0 0 2, and 0 0 3 reflections of the hydration product, respectively. All 0 0 *l* reflections are shifted to low angles by the hydration of pure WS_2 and the basal spacing (*d*) increases to 12.88 Å. The interlayer expansion (Δd) of 6.60 Å is due to a structure with bimolecular layers of water between WS_2 sheets [15], and also the 0 0 *l* reflection peaks in the pure WS_2 disappear completely, suggesting co-intercalation of water molecules with Li^+ into almost all interlayer spaces of WS_2.

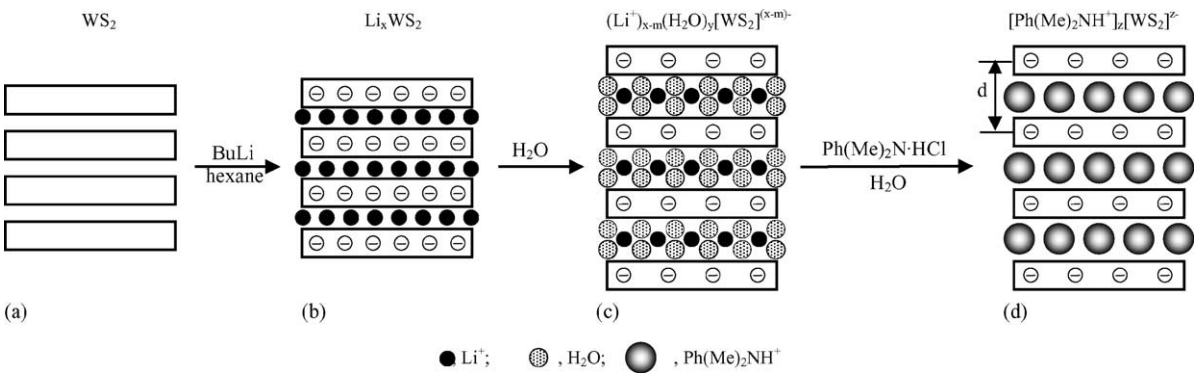

Scheme 1. Scheme of formation of *N,N*-dimethylanilinium ion intercalated WS_2: (a) WS_2, (b) lithium ion intercalated WS_2, (c) hydrated lithium ion intercalated WS_2 and (d) *N,N*-dimethylanilinium ion intercalated WS_2.

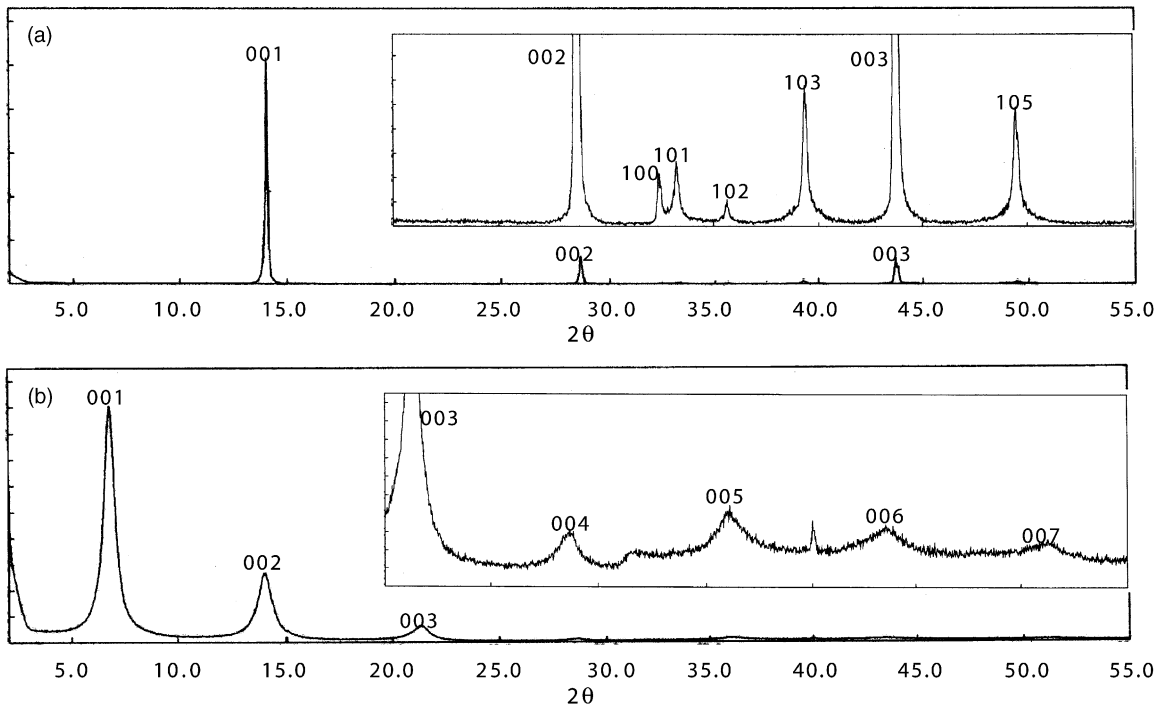

Fig. 1. XRD patterns of (a) pure WS_2 and (b) hydrated lithium ion intercalated WS_2.

The hydrated Li^+ present in the interlayer spaces was exchanged to $Ph(Me)_2NH^+$ by contacting the hydrated product with $Ph(Me)_2N{\cdot}HCl$ (Table 1), and the XRD pattern of the obtained product (TUN-1) in a dry state is shown in Fig. 2(a) together with that of $[Ph(Me)_2NH^+]_z[MoS_2]^{z-}$ (MON-1) (Fig. 2(b)) for comparison.

The peaks due to 0 0 1, 0 0 2, and 0 0 3 reflections for TUN-1 were observed at $2\theta = 8.62$, 17.46, and 26.48°, respectively. For MON-1 the peaks due to 0 0 1 and 0 0 2 reflections were observed at $2\theta = 7.38$ and 14.48°, respectively, but there was no peak due to 0 0 3 reflection, indicating that the crystallite size in the direction perpendicular to the basal plane of MON-1 was smaller than that of TUN-1. The 0 0 *l* reflections observed in pure WS_2 and pure MoS_2 were observed for neither TUN-1 nor MON-1. The 0 0 *l* reflections of TUN-1 are shifted to lower angles than those of pure WS_2 and the basal spacing (*d*) increased to be 10.25 Å. The interlayer difference (Δd) (3.97 Å) between pure WS_2 and TUN-1 was smaller compared with that (6.60 Å) between pure WS_2 and the hydrated product ($(Li^+)_{x-m}(H_2O)_y[WS_2]^{(x-m)-}$), indicating that a large amount of the hydrated cation, $Li^+(H_2O)_2$, present in the interlayer spaces of WS_2 were exchanged with $Ph(Me)_2NH^+$. The $Ph(Me)_2NH^+$ content in TUN-1 calculated from H (wt.%) is in good agreement with those calculated from C (wt.%) and N (wt.%), indicating that TUN-1 in a dry state does not contain water. No Li^+ could be detected in TUN-1 either by ICP measurement. These results indicate that only the $Ph(Me)_2NH^+$ is present in the interlayer spaces of TUN-1 and that the hydrated Li^+ is absent.

Table 1 summarizes results of XRD and elemental analysis for TUN-1 and MON-1.

The $Ph(Me)_2NH^+$ content ($z = 0.17$) per mol of WS_2 in TUN-1 is smaller than that ($z = 0.20$) per mol of MoS_2 in MON-1, and also, the interlayer difference ($\Delta d = 3.97$ Å) between pure WS_2 and TUN-1 is smaller than that ($\Delta d = 5.73$ Å) between pure MoS_2 and MON-1.

The basal plane of transition metal disulfide such as MoS_2 and WS_2 is composed of a monolayer of sulfur atoms; however, the edge surface is composed of one-dimensionally arranged sulfur atoms and transition metals such as Mo and W. Okuhara and coworker pointed out that the catalytic activity of MoS_2 for the isomerization of olefins such as 1-butene and *cis*-2-butene, which proceeds only on the edge site of MoS_2, increased with increasing edge site area resulting from a decrease in crystallite size in the direction

Table 1
Structural properties of $Ph(Me)_2NH^+$ intercalated WS_2 and MoS_2

No.	*d* (Å)	Δd (Å)	C (wt.%)	H (wt.%)	N (wt.%)	Composition
TUN-1	10.25	3.97	5.6	0.7	0.9	$[Ph(Me)_2NH^+]_{0.17}[WS_2]^{0.17-}$
MON-1	11.97	5.73	10.5	1.3	1.6	$[Ph(Me)_2NH^+]_{0.20}[MoS_2]^{0.20-}$

d = interlayer spacing. $\Delta d = d(Ph(Me)_2NH^+$ intercalated $MS_2) - d(MS_2)$. $d(MS_2) = 6.28$ (M: W), 6.24 (M: Mo).

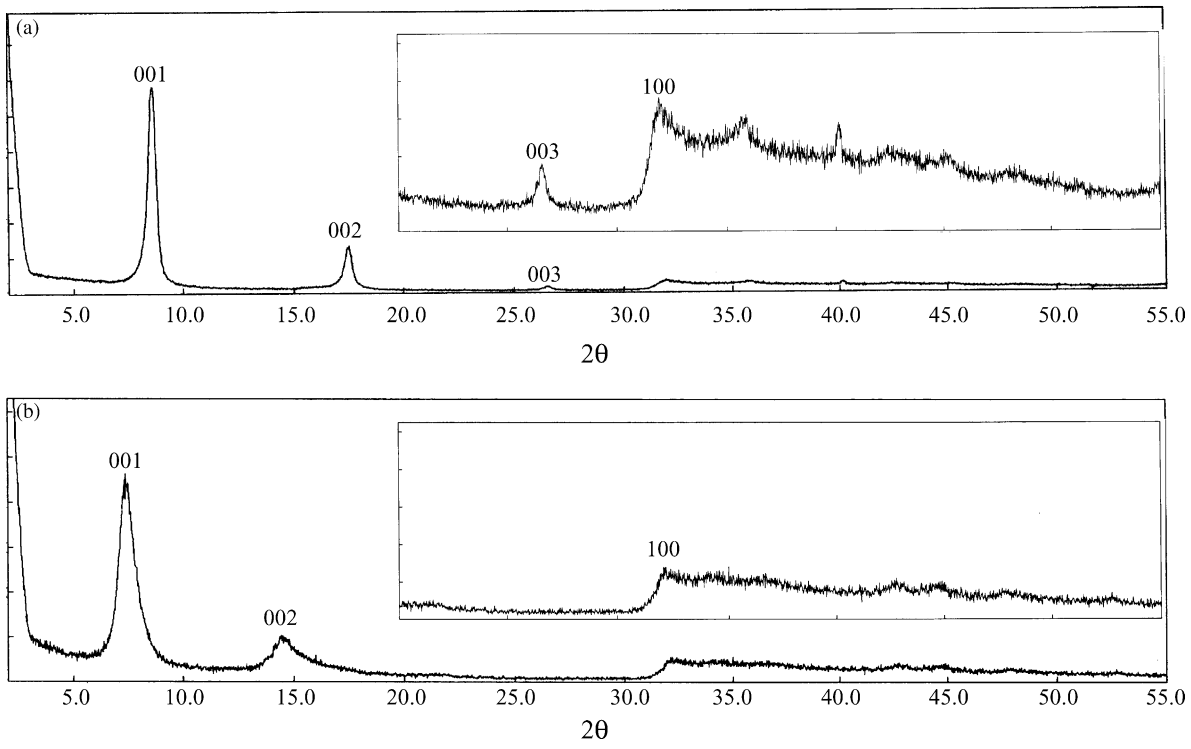

Fig. 2. XRD patterns of (a) $Ph(Me)_2NH^+$ intercalated WS_2 (TUN-1) and (b) $Ph(Me)_2NH^+$ intercalated MoS_2 (MON-1).

parallel to the basal plane of MoS_2 [18]. In the same way as MoS_2 for the olefin isomerization, only the edge sites of $[Ph(Me)_2NH^+]_z[WS_2]^{z-}$ and $[Ph(Me)_2NH^+]_z[MoS_2]^{z-}$ is considered to be effective for the activation of the metallocene catalysts. As the catalytic activities of $[Ph(Me)_2NH^+]_z[WS_2]^{z-}$ and $[Ph(Me)_2NH^+]_z[MoS_2]^{z-}$ would depend on both the $Ph(Me)_2NH^+$ content per mol of WS_2 or MoS_2 and their edge site areas, the crystallite sizes and the surface areas of TUN-1, MON-1, pure WS_2, and pure MoS_2 were measured and summarized in Table 2.

The crystallite sizes in the direction perpendicular to the basal plane and in the direction parallel to the basal plane were calculated by substituting the width of the 0 0 1 reflection peak and of the 1 0 0 reflection peak, respectively, for the Scherrer equation (Eq. (1)) [19]:

$$\text{crystallite size (Å)} = \frac{0.9\lambda}{\beta \cos\theta} \quad (1)$$

where λ is 1.5405 Å and β is the line width at half-height in radian, respectively. For TUN-1, the crystallite sizes were found to be 285 Å in the direction perpendicular to the basal plane and 180 Å in the direction parallel to the basal plane, respectively, and they are smaller than the corresponding values (310 and 320 Å) for pure WS_2 as a starting material. Calais et al. pointed out that for MoS_2 the smaller crystallite size led to the larger BET surface area [20]. The decrease in the crystallite size observed between pure WS_2 and TUN-1 led to the increase in the BET surface area. When compared

Table 2
X-ray, BET and XPS data for $Ph(Me)_2NH^+$ intercalated WS_2 and MoS_2

No.	X-ray hkl	2θ (Å)	β (rad)	Crystallite size (Å)	BET surface area (m^2/g)	XPS binding energy (eV)		
						W $4f_{7/2}$	Mo $3d_{5/2}$	S $2p_{3/2}$
TUN-1	0 0 1	8.62	0.49×10^{-2}	285	7.18	31.9		161.6
	1 0 0	31.90	0.80×10^{-2}	180				
WS_2	0 0 1	14.08	0.45×10^{-2}	310	2.51	33.0		162.6
	1 0 0	32.46	0.45×10^{-2}	320				
MON-1	0 0 1	7.38	0.94×10^{-2}	148	7.52		229.3	161.6
	1 0 0	32.12	1.29×10^{-2}	112				
MoS_2	0 0 1	14.40	0.49×10^{-2}	285	6.24		228.6	162.6
	1 0 0	32.66	0.45×10^{-2}	321				

Crystallite size $= 0.9\lambda/(\beta \cos\theta)$. $\lambda = 1.5405$ Å. β = linewidth at half-height.

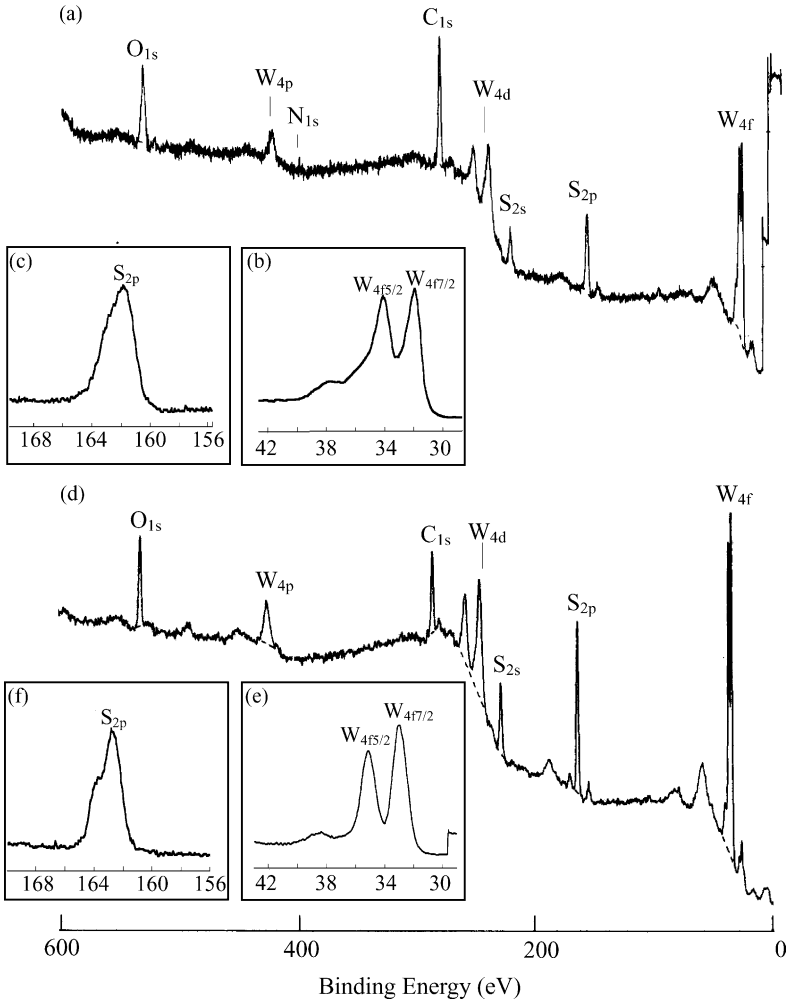

Fig. 3. XPS spectra of (a)–(c) $Ph(Me)_2NH^+$ intercalated WS_2 (TUN-1) and (d)–(f) pure WS_2.

with MON-1, TUN-1 had larger crystallite size and smaller BET surface area.

The reduction states of WS_2 in the TUN-1 were investigated by XPS, and the XPS spectra are shown in Fig. 3(a) and (d) for TUN-1 and pure WS_2, respectively.

In the spectrum of pure WS_2, peaks due to W 4p, W 4d, and W 4f were observed at the binding energies of 426, 243, and 33 eV, respectively, and those due to S 2s and S 2p at 226 and 163 eV, respectively. A peak due to O 1s was also observed at the binding energy of 532 eV, which is assigned to the O–W bond. In the spectrum of TUN-1, a very weak peak is observed at the binding energy of 403 eV, which is assigned to the N 1s, probably due to the presence of the $Ph(Me)_2NH^+$ intercalated into the interlayer spaces of WS_2. The expanded spectra at the W 4f region (30–42 eV) for TUN-1 and pure WS_2 are shown in Fig. 3(b) and (e), and also the corresponding spectra at the S 2p region (160–168 eV) are shown in Fig. 3(c) and (f), respectively. Table 2 also lists the binding energies for TUN-1 and pure WS_2, together with those for pure MoS_2 and MON-1 for comparison. The binding energies of both W 4f and S 2p in TUN-1 were low compared to those in WS_2. This suggests that electrons provided by BuLi exist not only on S in the intralayer of WS_2 but also on W. In the case of MON-1, a rise in the binding energy of Mo 3d and a drop in the binding energy of S 2p were observed in comparison with pure MoS_2. This suggests that electrons provided by BuLi into MoS_2 exist only on S atom in the intralayer of MoS_2 but do not on Mo atom, differently from the case of TUN-1. On the basis of these results, it is considered that the charge would be more delocalized on WS_2 in TUN-1 than on MoS_2 in MON-1.

To investigate the effect of the hydration conditions (time and temperature during soaking Li_xWS_2 in aqueous ammonia) on the catalyst structures, the $[Ph(Me)_2NH^+]_z[WS_2]^{z-}$ was prepared in various conditions (Table 3) and the results of XRD and XPS measurements are summarized in Table 4.

The basal spacing (d) values are virtually unchanged in the range of 10.11–10.25 Å regardless of the preparation conditions. However, the crystallite sizes are different depending on the conditions. The crystallite size decreased with time from 280 Å (30 min) to 190 Å (2 h and longer) in the direction perpendicular to the basal plane, and from 180 to 120 Å in the direction parallel to the basal plane. With increasing temperature from −30 to 0 °C, the crystallite size also

Table 3
Preparations of $Ph(Me)_2NH^+$ intercalated WS_2

No.	Reduction conditions				Hydration conditions			Ion exchange conditions		
	$[WS_2]$ (mol l^{-1})	[BuLi] (mol l^{-1})	Temperature (°C)	Time (h)	$[NH_3]$ (mol l^{-1})	Temperature (°C)	Time (h)	$[Ph(Me)_2N{\cdot}HCl]$ (mol l^{-1})	Temperature (°C)	Time (h)
TUN-1	0.3	1.6	105	18	13	−30	0.5	0.2	20	18
TUN-2	0.3	1.6	105	18	13	−30	2	0.2	20	18
TUN-3	0.3	1.6	105	18	13	−30	3	0.2	20	18
TUN-4	0.3	1.6	105	18	13	0	0.5	0.2	20	18

Solvents: hexane (reduction), water (hydration and ion exchange).

decreased from 280 to 90 Å in the direction perpendicular to the basal plane and from 180 to 110 Å in the direction parallel to the basal plane. The peaks due to W $4f_{7/2}$ and S $2p_{3/2}$ in $[Ph(Me)_2NH^+]_z[WS_2]^{z-}$ show almost the same binding energies in the range of 31.8–31.9 and 161.6–161.8 eV, respectively, regardless of the preparation conditions, but lower than the corresponding values (33.0 and 162.6 eV) in pure WS_2. The surface atomic ratios of the W, S, N, and O (O–W bond) in $[Ph(Me)_2NH^+]_z[WS_2]^{z-}$ were calculated on the basis of the their peak area at 31.8–31.9 (W $4f_{7/2}$), 161.6–161.8 (S $2p_{3/2}$), 531.0–531.2 (O 1s), and 402.4–402.6 eV (N 1s) in XPS spectra and are summarized in Table 4. The N/W ratio was 0 for pure WS_2 and almost 0.1 for $[Ph(Me)_2NH^+]_z[WS_2]^{z-}$ regardless of the hydration conditions. The constancy in the N/W ratio of $[Ph(Me)_2NH^+]_z[WS_2]^{z-}$ is also confirmed by no change in the binding energies of W $4f_{7/2}$ and S $2p_{3/2}$, indicating that the $Ph(Me)_2NH^+$/W ratio on the surface should be the same. The S/W ratios of TUN-1 and pure WS_2 were 2.0, indicating that the composition of the host compound (WS_2) is retained during the $Ph(Me)_2NH^+$ intercalation reactions involving the reduction, hydration, and ion exchange reactions. When this hydration reaction was carried out for longer time and at higher temperature, the S/W ratio decreased and the O/W ratio increased. This change in the S/W and O/W ratios indicates that only a part of sulfur atoms bound to tungsten atoms were replaced with oxygen atoms during the hydration reaction. Furimsky investigated the exchange reaction of WS_2 with oxygen, and found that the crystallite size of WS_2 might decrease during this reaction [21]. For $[Ph(Me)_2NH^+]_z[WS_2]^{z-}$ and pure WS_2, the relationships of the O/W ratio with the crystallite size are shown in Fig. 4.

The O/W ratio of $[Ph(Me)_2NH^+]_z[WS_2]^{z-}$ increased with a decrease in the crystallite size in directions both perpendicular and parallel to the basal plane.

To investigate the influence of the crystallite size of $[Ph(Me)_2NH^+]_z[WS_2]^{z-}$ on the reaction with a metallocene/alkylaluminum catalyst, loading of bis(indenyl)zirconium dichloride (Ind_2ZrCl_2)/triethylaluminum (Et_3Al) catalyst on $[Ph(Me)_2NH^+]_z[WS_2]^{z-}$ with different crystallite size was carried out. Ind_2ZrCl_2/Et_3Al catalyst solution in toluene was added to a slurry of $[Ph(Me)_2NH^+]_z[WS_2]^{z-}$ pretreated with Et_3Al in toluene and the mixture was stirred for 18 h at room temperature. The resulting $Ind_2ZrCl_2/Et_3Al/[Ph(Me)_2NH^+]_z[WS_2]^{z-}$ catalyst was permitted to stand for 3 days, the supernatant was removed, and then the precipitate was washed and dried to obtain supported Ind_2ZrCl_2/Et_3Al catalyst on $[Ph(Me)_2NH^+]_z[WS_2]^{z-}$. The reaction conditions and the results are summarized in Table 5. The

Table 4
X-ray and XPS data for $Ph(Me)_2NH^+$ intercalated WS_2

No.	XRD				Crystallite size (Å)	XPS				
	hkl	2θ (°)	d (Å)	β (rad)		Binding energy (eV)				Surface atomic ratio (W/S/N/O)
						W $4f_{7/2}$	S $2p_{3/2}$	O 1s	N 1s	
TUN-1	0 0 1	8.62	10.25	0.49×10^{-2}	280	31.9	161.6	531.0	402.6	1.0/2.0/0.1/0.4
	1 0 0	31.90		0.80×10^{-2}	180					
TUN-2	0 0 1	8.70	10.16	0.73×10^{-2}	190	31.9	161.6	531.0	402.3	1.0/1.9/0.1/0.5
	1 0 0	31.96		1.12×10^{-2}	130					
TUN-3	0 0 1	8.66	10.20	0.73×10^{-2}	190	31.5	161.3	531.0	401.8	1.0/1.9/0.1/0.5
	1 0 0	32.18		1.26×10^{-2}	120					
TUN-4	0 0 1	8.74	10.11	1.60×10^{-2}	90	31.9	161.8	531.2	402.5	1.0/1.9/0.1/0.6
	1 0 0	32.38		1.29×10^{-2}	110					
WS_2	0 0 1	14.08	6.28	0.45×10^{-2}	310	33.0	162.6	531.6	–	1.0/2.0/0.0/0.3
	1 0 0	32.46		0.45×10^{-2}	320					

d = interlayer spacing ($=\lambda/2\sin\theta$). $\lambda = 1.5405$ Å. $\Delta d = d(Ph(Me)_2NH^+$ intercalated $WS_2) - d(WS_2)$. β = linewidth at half-height. Crystallite size $= 0.9\lambda/(\beta\cos\theta)$.

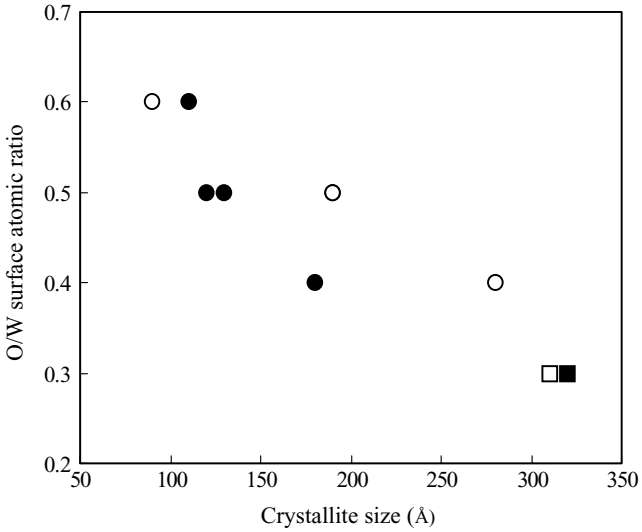

Fig. 4. O/W surface atomic ratio in XPS as a function of particle size in the direction perpendicular (○, □) and parallel (●, ■) to the basal plane for $Ph(Me)_2NH^+$ intercalated WS_2 and pure WS_2.

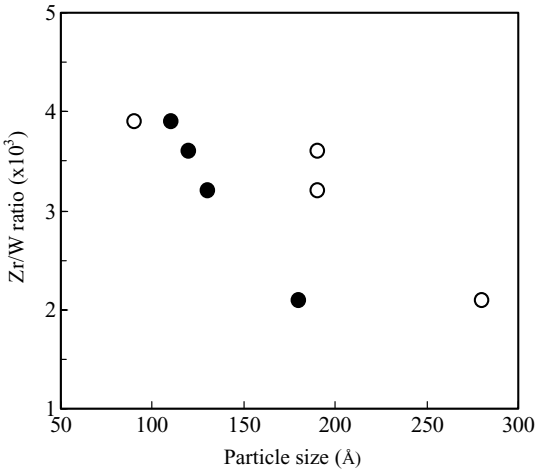

Fig. 5. Zr/W ratio in elemental analysis of the supported metallocene catalyst as a function of particle size in the direction perpendicular (○) and parallel (●) to the basal plane for $Ph(Me)_2NH^+$ intercalated WS_2.

zirconium loadings in the supported Ind_2ZrCl_2/Et_3Al catalyst (ZTUN-1–ZTUN-4) obtained were determined by ICP measurement to be 0.06–0.11 wt.%, indicating that the Ind_2ZrCl_2/Et_3Al catalyst was supported on $[Ph(Me)_2NH^+]_z[WS_2]^{z-}$.

Fig. 5 shows the relationship of the crystallite sizes in $[Ph(Me)_2NH^+]_z[WS_2]^{z-}$ with the Zr/W ratios in the supported Ind_2ZrCl_2/Et_3Al catalyst. The Zr/W ratio increased with a decrease in the crystallite size in $[Ph(Me)_2NH^+]_z[WS_2]^{z-}$, suggesting that the loadings of the Ind_2ZrCl_2/Et_3Al catalyst on $[Ph(Me)_2NH^+]_z[WS_2]^{z-}$ increased with an increase in edge site area accompanying a decrease in the crystallite size in the direction parallel to the basal plane.

3.2. Ethylene polymerization with the metallocene catalyst activated with $Ph(Me)_2NH^+$ intercalated WS_2

Ethylene polymerization was carried out in the presence of Ind_2ZrCl_2/Et_3Al catalysts activated with $[Ph(Me)_2NH^+]_z[WS_2]^{z-}$ ($Ind_2ZrCl_2/Et_3Al/[Ph(Me)_2NH^+]_z[WS_2]^{z-}$ catalyst) at 80 °C under ethylene pressure of 0.6 MPa or 2.0 MPa to investigate their potential as ethylene polymerization catalysts. The results of the ethylene polymerization by the Ind_2ZrCl_2/Et_3Al catalyst activated with TUN-1 in various amounts, which has the largest crystallite size, are summarized in Table 6 together with the results obtained by pure WS_2 and MON-1.

Addition of TUN-1 into the Ind_2ZrCl_2/Et_3Al (1 μmol/500 μmol) catalyst enhanced the catalytic activity drastically (nos. 1 and 3) compared with the addition of WS_2 in almost the same amount (no. 2). These results indicate that TUN-1 is significantly effective as a cocatalyst for the Ind_2ZrCl_2/Et_3Al catalyst. Poly(ethylene) produced by the Ind_2ZrCl_2/Et_3Al/TUN-1 catalyst had the molecular weight (M_n) as large as that obtained by the Ind_2ZrCl_2/Et_3Al catalyst and its polydispersity (M_w/M_n) index was 2.3, being consistent with the features of polymers produced with metallocene catalysts [22]. This indicates that the cationic monoalkylmetallocene Ind_2ZrR^+ as an active species was supported structurally intact on the two-dimensional macroanion of WS_2 [23]. The catalytic activity per mmol of Ind_2ZrCl_2 and per hour of the Ind_2ZrCl_2/Et_3Al/MON-1 catalyst increased with an increase in the MON-1 charge (nos. 4–6, ethylene 2.0 MPa). The same trend was observed with the Ind_2ZrCl_2/Et_3Al/TUN-1 catalyst (nos. 7–9, ethylene 0.6 MPa). Based on results shown in Table 6 (no.

Table 5
Preparation and Zr/W ratio of the supported $Ind_2ZrCl_2/AlEt_3$ catalysts on various $Ph(Me)_2NH^+$ intercalated WS_2

No.	Reaction conditions				Products		
	Ind_2ZrCl_2 (μmol)	$[Ph(Me)_2NH^+]_z[WS_2]^{z-}$		$AlEt_3$ (mmol)	W (wt.%)	Zr (wt.%)	Zr/W
		No.	(mg)				
ZTUN-1	10.1	TUN-1	775	3	56.8	0.06	2.1×10^{-3}
ZTUN-2	10.0	TUN-2	770	3	56.6	0.09	3.2×10^{-3}
ZTUN-3	10.0	TUN-3	775	3	56.8	0.10	3.6×10^{-3}
ZTUN-4	10.1	TUN-4	790	3	57.1	0.11	3.9×10^{-3}

Reaction conditions: toluene, 100 ml; temperature, 20 °C; time, 18 h.

Table 6
Ethylene polymerizations with the $Ind_2ZrCl_2/AlEt_3$ catalysts activated with $Ph(Me)_2NH^+$ intercalated WS_2 and MoS_2

Run no.	$[Ph(Me)_2NH^+]_z[MS_2]^{z-}$					P_e[a] (MPa)	Time (min)	Yield (g)	Activity (kg/(mmol Zr h))	M_n ($\times10^{-4}$)	M_w/M_n
	No.	M	z	(mg)	$Ph(Me)_2NH^+$ (μmol)						
1				0.0	0	2.0	60	18	18	27	2.3
2	WS_2	W	0	75.0	0	2.0	60	16	16		
3	TUN-1	W	0.17	78.5	48.7	2.0	17	121	427	23	2.3
4	MON-1	Mo	0.21	26.9	30.1	2.0	60	24	24	19	2.2
5	MON-1	Mo	0.21	59.9	67.1	2.0	60	56	56		
6	MON-1	Mo	0.21	134.4	150.5	2.0	60	127	127	14	2.1
7	TUN-1	W	0.17	31.5	19.6	0.6	60	75	75		
8	TUN-1	W	0.17	75.1	46.6	0.6	60	151	151		
9	TUN-1	W	0.17	130.0	80.7	0.6	60	165	165		
10	MON-1	Mo	0.21	129.7	145.3	0.6	60	25	25		

Polymerization conditions: toluene, 500 ml; Ind_2ZrCl_2, 1.0 μmol; $AlEt_3$, 500 μmol; temperature, 80 °C.
[a] Ethylene pressure.

3 versus no. 6, and no. 9 versus no. 10), it is clear that TUN-1 is more suitable for the activator than MON-1. The activity of the Ind_2ZrCl_2/Et_3Al/TUN-1 catalyst drastically increased when the $Ph(Me)_2NH^+$ content was increased from 20 to 47 μmol and then slightly increased when it was further increased to 81 μmol (nos. 7–9, Ind_2ZrCl_2 1 μmol, ethylene 0.6 MPa), indicating that the $Ph(Me)_2NH^+$ content more than 47 μmol is necessary to activate the Ind_2ZrCl_2/Et_3Al catalyst (1 μmol/500 μmol) and that only a part of $Ph(Me)_2NH^+$ present in the interlayer spaces of WS_2 could contribute to the activation of the Ind_2ZrCl_2/Et_3Al catalyst. The crystallite size in the direction parallel to the basal plane (180 Å) for TUN-1 is larger than that (112 Å) for MON-1 as shown in Table 2, indicating that the edge site area for TUN-1 is smaller than that for MON-1. The $Ph(Me)_2NH^+$ content (0.17) in TUN-1 is smaller than that (0.20) in MON-1 as shown in Table 1. It is therefore considered that the $Ph(Me)_2NH^+$ content on the edge site of TUN-1 is less than that of MON-1. However, the catalytic activity of TUN-1 at the total $Ph(Me)_2NH^+$ content of 20 μmol was three times higher than that of MON-1 at the total $Ph(Me)_2NH^+$ content of 145 μmol as shown in Table 6 (no. 7 versus no. 10). We, therefore, investigated the influence of the crystallite sizes on the catalytic activity of the $Ind_2ZrCl_2/Et_3Al/[Ph(Me)_2NH^+]_z[WS_2]^{z-}$ catalyst, and the results are shown in Table 7.

The decrease in the crystallite sizes with the $Ph(Me)_2NH^+/W$ ratio (N/W = 0.1) constant on the surface (by XPS measurement) would lead to an increase in the total $Ph(Me)_2NH^+$ content on the edge site and would increase the catalytic activity of $[Ph(Me)_2NH^+]_z[WS_2]^{z-}$. However, the catalytic activity per mmol of Ind_2ZrCl_2 and per hour at $[Ph(Me)_2NH^+]_z[WS_2]^{z-}$ of 75 mg decreased drastically with a decrease in the crystallite sizes of $[Ph(Me)_2NH^+]_z[WS_2]^{z-}$. TUN-4 having crystallite size (110 Å) in the direction parallel to the basal plane approximately the same as that (112 Å) of MON-1 (no. 4 in Table 7) gave rise to a low level of catalytic activity similar to the Ind_2ZrCl_2/Et_3Al/MON-1 catalyst (no. 10 in Table 6). It is considered that the difference in the catalytic activity between the Ind_2ZrCl_2/Et_3Al/TUN-1 catalyst and the Ind_2ZrCl_2/Et_3Al/MON-1 catalyst would result from the difference in the crystallite sizes in the direction parallel to the basal plane rather than the difference in the $Ph(Me)_2NH^+$ content (Table 1) and the reduction state (Table 2).

3.3. Ethylene polymerization with the supported Ind_2ZrCl_2/Et_3Al catalyst on the $Ph(Me)_2NH^+$ intercalated WS_2

To understand the effect of the crystallite sizes on the catalytic activities of the $Ind_2ZrCl_2/Et_3Al/[Ph(Me)_2NH^+]_z$

Table 7
Ethylene polymerizations with the $Ind_2ZrCl_2/AlEt_3$ catalysts activated with various $Ph(Me)_2NH^+$ intercalated WS_2

Run no.	Ind_2ZrCl_2 (μmol)	$[Ph(Me)_2NH^+]_z[MS_2]^{z-}$				Activity	
		No.	Crystallite size (Å)		(mg)	(kg/(mmol Zr h))	(kg/(g $[Ph(Me)_2NH^+]_z[MS_2]^{z-}$ h))
			001	100			
1	1.0	TUN-1	280	180	75.1	151	2.0
2	1.0	TUN-2	190	130	75.0	105	1.4
3	1.0	TUN-3	190	120	75.2	99	1.3
4	1.0	TUN-4	90	110	75.1	25	0.3

Polymerization conditions: toluene, 500 ml; $AlEt_3$, 500 μmol; ethylene, 0.6 MPa; temperature, 80 °C; time, 1 h.

Table 8
Ethylene polymerizations with the supported $Ind_2ZrCl_2/AlEt_3$ catalysts on various $Ph(Me)_2NH^+$ intercalated WS_2

Run no.	Supported catalyst			Activity	
	No.	(mg)	Zr (μmol)	(kg/(mmol Zr h))	(kg/[g (supported catalyst) h])
1	ZTUN-1	75.1	0.49	230	1.5
2	ZTUN-2	75.2	0.74	71	0.7
3	ZTUN-3	75.2	0.82	55	0.6
4	ZTUN-4	75.0	0.90	17	0.2

Polymerization conditions: toluene, 500 ml; $AlEt_3$, 300 μmol; ethylene, 0.6 MPa; temperature, 80 °C; time, 1 h.

$[WS_2]^{z-}$ catalyst, the ethylene polymerization with Ind_2ZrCl_2/Et_3Al catalysts supported on $[Ph(Me)_2NH^+]_z[WS_2]^{z-}$ in different crystallite sizes was carried out at 80 °C under the ethylene pressure of 0.6 MPa and the results are summarized in Table 8.

The supported Ind_2ZrCl_2/Et_3Al catalyst, which is the precipitate of $Ind_2ZrCl_2/Et_3Al/[Ph(Me)_2NH^+]_z[WS_2]^{z-}$ catalyst, was effective as the ethylene polymerization catalyst, but the supernatant solution showed no activity. This indicates that the active species of the $Ind_2ZrCl_2/Et_3Al/[Ph(Me)_2NH^+]_z[WS_2]^{z-}$ catalyst would be the cationic monoalkylmetallocene, that is, the Ind_2ZrR^+ adsorbed on the edge site of $[Ph(Me)_2NH^+]_z[WS_2]^{z-}$.

Fig. 6 shows the relationships between the crystallite sizes of $[Ph(Me)_2NH^+]_z[WS_2]^{z-}$ and the catalytic activities per gram of the supported catalyst and per hour.

The Zr/W mol ratio (by ICP measurement) in the bulk of the supported catalyst increased with a decrease in crystallite sizes of the $[Ph(Me)_2NH^+]_z[WS_2]^{z-}$, suggesting that the amount of the Ind_2ZrCl_2/Et_3Al catalyst adsorbed on the edge site of the $[Ph(Me)_2NH^+]_z[WS_2]^{z-}$ would increase with the decrease in the crystallite sizes in the direction parallel to the basal plane of the $[Ph(Me)_2NH^+]_z[WS_2]^{z-}$. However, the catalytic activity decreased drastically with the decrease in the crystallite sizes. These results suggest that not only the active species, namely, Ind_2ZrR^+ but also the inactive species for ethylene polymerization are contained in the Ind_2ZrCl_2/Et_3Al catalyst adsorbed on the edge site of $[Ph(Me)_2NH^+]_z[WS_2]^{z-}$ and the latter fraction would increase drastically with the decrease in the crystallite size in the direction parallel to the basal plane of $[Ph(Me)_2NH^+]_z[WS_2]^{z-}$. Jordan et al. reported that isolated base-coordinated complexes of the type $[Cp_2MR^+(THF)][BPh_4^-]$ (M: Ti, Zr; R: CH_3, CH_2Ph) polymerize ethylene very slowly due to the presence of a Lewis base [24]. We speculate that the inactive species would be the base-coordinated adducts of the type $Ind_2Zr(R)$-O-WS-$(WS_2)_\infty$. This speculation is supported by the increase in the O/W ratio of $[Ph(Me)_2NH^+]_z[WS_2]^{z-}$ revealed by XPS measurement with the decrease in the crystallite size as shown in Fig. 4.

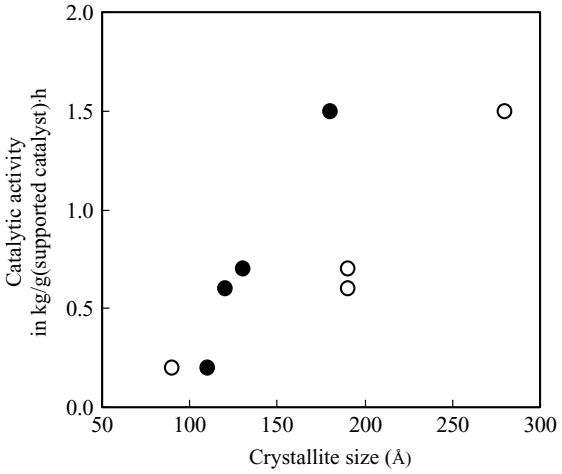

Fig. 6. Catalytic activity as a function of crystallite size in the direction perpendicular (○) and parallel (●) to the basal plane for $[Ph(Me)_2NH^+]_z[WS_2]^{z-}$ for ethylene polymerization with the supported Ind_2ZrCl_2/Et_3Al catalysts on $[Ph(Me)_2NH^+]_z[WS_2]^{z-}$.

4. Conclusion

Synthesis of $Ph(Me)_2NH^+$ salts of anion obtained by "topotactic" reduction of WS_2 with BuLi, the effect of these compounds as a cocatalyst of Ind_2ZrCl_2/Et_3Al in ethylene polymerization, and the influence of crystallite size of the cocatalyst for the ethylene polymerization were investigated in comparison with MoS_2-based cocatalyst. Li^+ intercalated in interlayer space of WS_2 by "topotactic" reduction of WS_2 with BuLi was hydrated and then exchanged with $Ph(Me)_2NH^+$. In ethylene polymerization, addition of this $Ph(Me)_2NH^+$ intercalated WS_2 ($[Ph(Me)_2NH^+]_z[WS_2]^{z-}$) to the Ind_2ZrCl_2/Et_3Al catalyst enhanced drastically the catalytic activity in comparison with the $Ph(Me)_2NH^+$ intercalated MoS_2 ($[Ph(Me)_2NH^+]_z[MoS_2]^{z-}$). Poly(ethylene) obtained with the $Ind_2ZrCl_2/Et_3Al/[Ph(Me)_2NH^+]_z[WS_2]^{z-}$ catalyst had typical features such as narrow molecular weight distribution like polymers obtained with conventional metallocene catalysts, indicating that the active species of this catalyst system was the cationic monoalkylmetallocene (Ind_2ZrR^+) adsorbed on the edge site of the $[Ph(Me)_2NH^+]_z[WS_2]^{z-}$. The Zr loadings of the $Ind_2ZrCl_2/Et_3Al/[Ph(Me)_2NH^+]_z[WS_2]^{z-}$ catalyst increased with the decrease in the crystallite size of the $[Ph(Me)_2NH^+]_z[WS_2]^{z-}$. However, simultaneously the catalytic activity of the catalyst decreased drastically, indicating that the decrease of the crystallite size led to the

significant increase of inactive species for ethylene polymerization, probably the base-coordinated adducts. For the effect of the crystallite size of the cocatalysts based on two-dimensional host lattice systems other than WS_2 such as MoS_2, TaS_2, and TiS_2 for ethylene polymerization, a more detailed study is now being carried out, and the results will be published elsewhere.

Acknowledgements

The authors thank Prof. S. Yamanaka, Department of Applied Chemistry, Faculty of Engineering, Hiroshima University for helpful discussions and TOSOH Analysis and Research Center for the analysis of the cocatalyst.

References

[1] H. Sinn, W. Kaminsky, Adv. Organomet. Chem. 18 (1980) 99.
[2] W. Kaminsky, M. Miri, H. Sinn, R. Woldt, Makromol. Chem. Rapid Commun. 4 (1983) 417.
[3] P.G. Gassman, M.R. Callstrom, J. Am. Chem. Soc. 109 (1987) 7875.
[4] C. Sishta, R.M. Hathorn, T.J. Marks, J. Am. Chem. Soc. 114 (1992) 1112.
[5] R.F. Jordan, W.E. Dasher, S. Echols, J. Am. Chem. Soc. 108 (1986) 1718.
[6] Z. Lin, J.-F. Le Marechal, M. Sabat, T.J. Marks, J. Am. Chem. Soc. 109 (1987) 4127.
[7] H.W. Turner, G.G. Hlatky, PCT Int. Appl. WO 91/14713, 1991.
[8] J.C.W. Chien, W.M. Tsai, Makromol. Chem., Macromol. Symp. 66 (1993) 141.
[9] X. Yang, C.L. Stern, T.J. Marks, Organometallics 10 (1991) 840.
[10] N. Herfert, G. Fink, Makromol. Chem. Rapid Commun. 14 (1993) 91.
[11] R. Schöllhorn, Angew. Chem. Int. Ed. Engl. 19 (1980) 983.
[12] S. Yamada, A. Yano, US Patent 6,372,681 (2002).
[13] S. Yamada, A. Yano, M. Sato, T. Itoh, J. Mol. Catal. A: Chem. 200 (2003) 239.
[14] E. Samuel, J. Organomet. Chem. 4 (1965) 156.
[15] R.F. Frindt, D. Yang, Mol. Cryst. Liquid Cryst. 311 (1998) 367.
[16] R. Schöllhorn, A. Weiss, J. Less-Common Met. 36 (1974) 229.
[17] M.S. Whittingham, Prog. Solid State Chem. 12 (1978) 41.
[18] K. Tanaka, T. Okuhara, J. Catal. 78 (1982) 155.
[19] T.A. Pecoraro, R.R. Chianelli, J. Catal. 67 (1981) 430.
[20] C. Calais, N. Matsubayashi, C. Geantet, Y. Yoshimura, H. Shimada, A. Nishijima, M. Lacroix, M. Breysse, J. Catal. 174 (1998) 130.
[21] E. Furimsky, Catal. Rev. Sci. Eng. 22 (3) (1980) 371.
[22] W. Kaminsky, M. Miri, H. Sinn, R. Woldt, Makromol. Chem. Rapid Commun. 4 (1983) 417.
[23] M. Kaminaka, K. Soga, Makromol. Chem. Rapid Commun. 12 (1991) 367.
[24] R.F. Jordan, C.S. Bajgur, R. Willett, B. Scott, J. Am. Chem. Soc. 108 (1986) 7410.